International Journal of
Molecular Sciences

MDPI

Article

Aggravation of TGFβ1-Smad Pathway and Autoimmune Myocarditis by Fungicide (Tebuconazole) Exposure

Ylenia Marino [1,†], Alessia Arangia [1,†], Ramona D'Amico [1], Marika Cordaro [2], Rosalba Siracusa [1], Daniela Impellizzeri [1], Enrico Gugliandolo [3], Roberta Fusco [1,*], Salvatore Cuzzocrea [1,‡] and Rosanna Di Paola [3,‡]

1 Department of Chemical, Biological, Pharmaceutical and Environmental Sciences, University of Messina, 98166 Messina, Italy; ylenia.marino@studenti.unime.it (Y.M.)
2 Department of Biomedical, Dental and Morphological and Functional Imaging, University of Messina, Consolare Valeria, 98100 Messina, Italy
3 Department of Veterinary Sciences, University of Messina, 98168 Messina, Italy
* Correspondence: rfusco@unime.it
† These authors contributed equally to this work.
‡ These authors also contributed equally to this work.

Abstract: Myocarditis is an inflammatory cardiac disorder and the primary cause of heart failure in young adults. Its origins can be attributed to various factors, including bacterial or viral infections, exposure to toxins or drugs, endocrine disruptors (EDs), and autoimmune processes. Tebuconazole (TEB), which is a member of the triazole fungicide family, is utilized to safeguard agricultural crop plants against fungal pathogens. Although TEB poses serious threats to mammal health, the information about how it induces toxic effects through various pathways, particularly in autoimmune diseases, are still limited. Thus, the aim of this paper was to evaluate the effect of TEB exposure in autoimmune myocarditis (AM). To induce AM, rats were immunized with porcine cardiac myosin and exposed to TEB for 21 days. Thereafter, animals were sacrificed, and histological, biochemical, and molecular analyses were performed. TEB exposure increased heart weight, systolic blood pressure and heart rate already augmented by AM. Additionally, it significantly increased creatine phosphokinase heart (CK-MB), creatine phosphokinase (CPK), cardiac troponin T (cTnT), and cardiac troponin I (cTnI), as compared to the control. From the histological perspective, TEB exacerbates the histological damage induced by AM (necrosis, inflammation and cell infiltration) and increased fibrosis and collagen deposition. TEB exposure strongly increased pro-inflammatory cytokines and prooxidant levels ($O2^-$, H_2O_2, NO_2^-, lipid peroxidation) and reduced antioxidant enzyme levels, which were already dysregulated by AM. Additionally, TEB increased NOX-4 expression and the TGFβ1-Smads pathway already activated by AM. Overall, our results showed that TEB exposure strongly aggravated the cardiotoxicity induced by AM.

Keywords: myocarditis; fungicide; animal model

check for updates

Citation: Marino, Y.; Arangia, A.; D'Amico, R.; Cordaro, M.; Siracusa, R.; Impellizzeri, D.; Gugliandolo, E.; Fusco, R.; Cuzzocrea, S.; Di Paola, R. Aggravation of TGFβ1-Smad Pathway and Autoimmune Myocarditis by Fungicide (Tebuconazole) Exposure. *Int. J. Mol. Sci.* **2023**, *24*, 11510. https://doi.org/10.3390/ijms241411510

Academic Editors: Christophe Chevillard and Buddhadeb Dawn

Received: 3 April 2023
Revised: 29 June 2023
Accepted: 14 July 2023
Published: 15 July 2023

Copyright: © 2023 by the authors. Licensee MDPI, Basel, Switzerland. This article is an open access article distributed under the terms and conditions of the Creative Commons Attribution (CC BY) license (https://creativecommons.org/licenses/by/4.0/).

1. Introduction

Myocarditis is a condition that involves inflammation of the heart and is characterized by the presence of nonischemic inflammatory infiltrates within the heart tissue. This inflammation can cause damage to the cardiomyocytes, leading to necrosis and/or degeneration. The causes of myocarditis have been attributed to various factors, including viral or bacterial infections, the usage of drugs or toxins or endocrine disruptors (EDs), and autoimmune processes. Inflammation of the myocardium can progress from an acute phase to subacute and chronic phases. This can ultimately result in tissue remodeling, damage to the architecture of the myocardium, fibrosis, and depressed contractility [1]. Giant cell myocarditis, which is a form of autoimmune myocarditis (AM), is often linked with a poor prognosis. This is because it can frequently progress to dilated cardiomyopathy

(DCM) during the chronic stages. Research suggests that around one-third of cases of autoimmune myocarditis result in heart failure. Additionally, nearly 40% of all instances of heart failure in individuals under the age of 40 are thought to be linked to autoimmune myocarditis [2]. Exposure to EDs has risen in recent times, which has led to growing concern regarding the impact of these chemicals on human health. They are frequently present in the environment and are primarily derived from industrial and agricultural sources [3]. These sources include pesticides, herbicides, and various chemicals utilized in the plastics industry and in consumer products. EDs have become a subject of interest in human physiopathology because they have the potential to disrupt the endocrine and immune systems [4,5]. Tebuconazole (TEB) [(RS)-1-p-chlorophenyl-4,4-dimethyl-3-(1H-1,2,4-triazol-1-yl methyl)pentan-3-ol] is a highly effective fungicide that is widely used due to its potent antifungal properties. TEB is a member of the triazole family of compounds that are known to inhibit the activity of lanosterol-14-α-demethylase (cytochrome P450) in fungi. This inhibition results in the arrest of fungal ergosterol synthesis, which, in turn, disrupts cell membrane integrity and inhibits fungal growth [6]. Nevertheless, the strong fungicidal properties of triazole fungicides can also affect several pathways in non-target organisms, leading to various adverse effects. Several ecotoxicological studies have shown that TEB is extensively used during the growing season, leading to its detection in various environmental areas [7]. TEB residues have been detected in humans, specifically in urine and hair samples from farm workers, with concentrations of 19.2 µg/L and 2.22 ng/kg, respectively [8,9]. The improper use and abuse of triazole fungicides has become a growing public concern due to their potential health and environmental impacts. These compounds have been found to cause harmful effects on both animals and humans. In fact, the United States Environmental Protection Agency has classified TEB as such. Although frequent exposure to TEB poses a risk, there is a limited amount of research on the toxic effects of this fungicide in mammals. It has been already demonstrated that TEB exposure induces cardiotoxic effects after chronic exposure [10]. In this study, it was observed that TEB led to a decrease in cardiac acetylcholinesterase, an increase in serum marker enzymes such as creatinine phosphokinase (CPK) and lactate dehydrogenase (LDH), and modifications in the lipid profile. These changes included elevated levels of total cholesterol (T-CHOL), triglyceride (TG), low-density lipoprotein cholesterol (LDL-C), and reduced levels of high-density lipoprotein cholesterol (HDL-C) in the serum. Moreover, TEB resulted in elevated levels of p53 and the Bax/Bcl2 ratio, released cytochrome c into the cytosol, and triggered the activation of caspase-9 and caspase-3. In addition, the findings indicated that TEB caused genotoxic effects, including DNA fragmentation and an increased frequency of micronucleated bone marrow cells. Furthermore, TEB exposure led to the development of myocardial fibrosis. These results imply that exposure to TEB can induce apoptosis. Recently, several authors described the role of Eds in autoimmune diseases [11,12] but no data are available on TEB's role in autoimmune myocarditis. Thus, this study aims to examine the impact the exposure to TEB on the histopathological changes in adult male rats subjected to AM.

2. Results

2.1. TEB Exposure Increased Systolic Blood Pressure and Heart Rate Induced by AM

To preliminarily verify the effect of TEB exposure on rats subjected to AM, body weight (Bw) and heart weight (Hw) were recorded. TEB exposure did not affect Bw either in control or AM rats. However, TEB exposure increased Hw in control and AM animals. Consequently, the Hw/Bw ratio was found to be increased in AM ($p = 0.0305$) and AM + TEB animals ($p < 0.0001$) as compared to control, and the two groups were statistically different ($p = 0.0179$) (Figure 1A). AM significantly increased systolic blood pressure (SBP) ($p = 0.0008$) (Figure 1B), without affecting diastolic blood pressure (DBP) (Figure 1C) and increasing the heart rate ($p = 0.0151$) (HR) (Figure 1D), as compared to control. TEB exposure also increased SBP (Figure 1B) in both control ($p = 0.203$) and AM animals ($p = 0.0253$) and the HR ($p = 0.0137$ and $p = 0.0032$, respectively) (Figure 1D) as well,

while not affecting di DBP (Figure 1C). AM significantly increased creatine phosphokinase heart (CK-MB) (Figure 1E, $p < 0.0001$), creatine phosphokinase (CPK) (Figure 1F, $p < 0.0001$), cardiac troponin T (cTnT) (Figure 1G, $p < 0.0001$), and cardiac troponin I (cTnI) (Figure 1H, $p < 0.0001$), as compared to control. TEB exposure further increased all these parameters in both control (Figure 1E, $p = 0.0303$, Figure 1F, $p = 0.0199$, Figure 1G, $p = 0.0019$, Figure 1H, $p = 0.0382$ respectively) and AM animals (Figure 1E, $p < 0.0001$, Figure 1F, $p = 0.0026$, Figure 1G, $p = 0.0025$, Figure 1H, $p = 0.0003$ respectively).

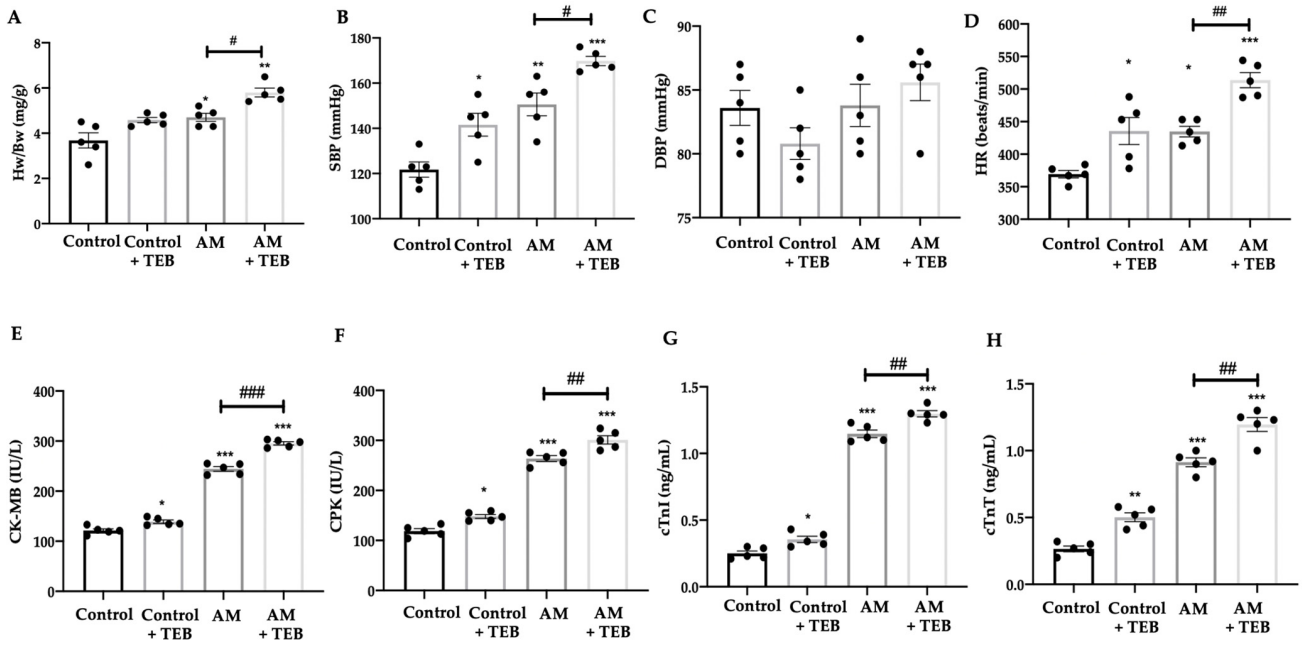

Figure 1. Effect of TEB exposure on body and heart weight and blood pressure in AM-induced animals: (**A**) TEB exposure increased heart weight (Hw)/body weight (Bw) ratio in animals subjected to AM; (**B**) TEB exposure increased systolic blood pressure (SBP) in both control and AM groups; (**C**) diastolic blood pressure (DBP) was not affected by TEB exposure; (**D**) heart rate (HR) was significantly increased by TEB exposure in control and AM groups. TEB exposure increased (**E**) creatine phosphokinase heart (CK-MB), (**F**) creatine phosphokinase (CPK), (**G**) cardiac troponin T (cTnT), and (**H**) cardiac troponin I. Results were analyzed by one-way ANOVA, followed by a Bonferroni post hoc test for multiple comparisons. A *p*-value of less than 0.05 was considered significant. * $p < 0.05$ vs. Control, # $p < 0.05$ vs. AM, ** $p < 0.01$ vs. control, ## $p < 0.01$ vs. AM, *** $p < 0.001$ vs. control, ### $p < 0.001$ vs. AM.

2.2. TEB Exposure Aggravates Myocardial Damage Induced by AM

Hematoxylin and eosin staining was performed to evaluate the myocardial damage. Control + TEB group showed necrosis, edema and cellular infiltration (Figure 2B,E, $p = 0.0192$ and Figure 2F, $p = 0.0192$, Figure S1B), as compared to the control group (Figures 2A,E,F and S1A). Animals subjected to AM showed a significant myocardial injury (Figure 2C,E, $p = 0.0017$ and Figure 2F, $p < 0.0001$, Figure S1C), which was significantly increased in AM animals exposed to TEB (Figure 2D,E, $p < 0.0001$ and Figure 2F, $p < 0.0001$, Figure S1D), as compared to the control. AM and AM + TEB groups were statistically different (Figure 2E, $p = 0.0192$ and Figure 2F, $p = 0.0005$, Figure S1). TUNEL assay was performed to evaluate apoptosis (Figure S2). An increased number of TUNEL-positive cells were detected in the AM group (Figure S2C,E), as compared to control (Figure S2A,E, $p < 0.0001$). TEB exposure strongly increased TUNEL-positive cells in both control (Figure S2B,E, $p = 0.004$) and AM groups (Figure S2D,E, $p = 0.0006$).

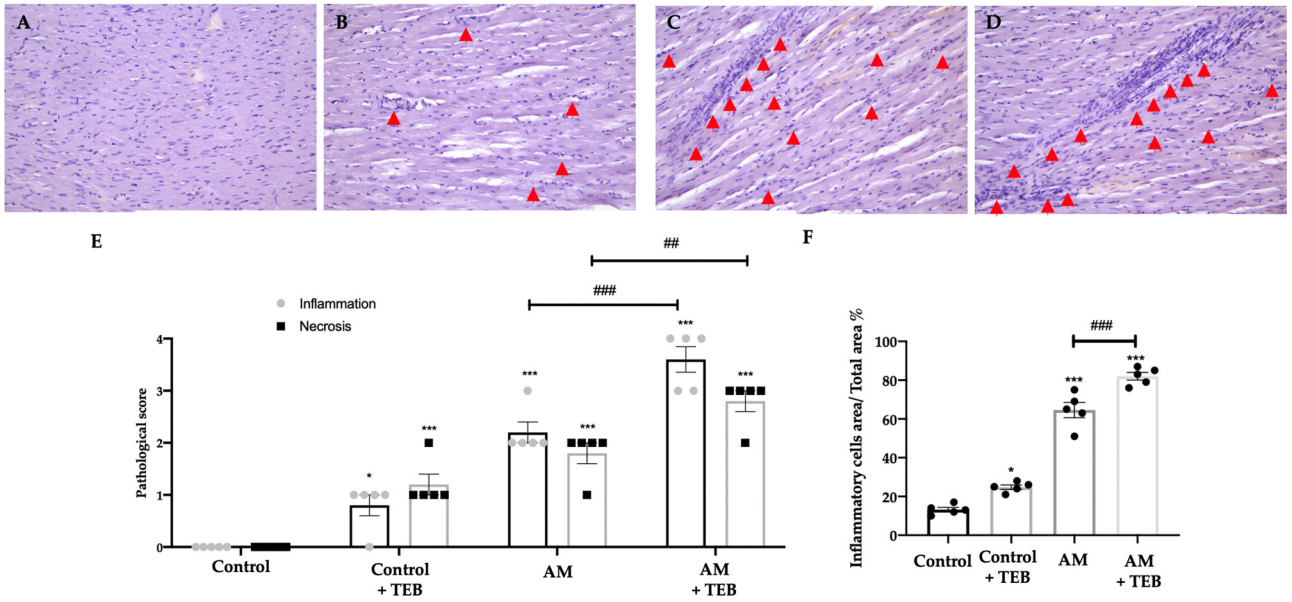

Figure 2. Effect of TEB exposure on histological damage induced by AM: Hematoxylin and eosin staining of: (**A**) control, (**B**) control + TEB, (**C**) AM, (**D**) AM + TEB groups showed that TEB exposure increased the (**E**) pathological score of both control and AM group. In the same groups TEB exposure increased the (**F**) inflammatory cells infiltration score. Arrows indicated the infiltrating area. Results were analyzed by one-way ANOVA, followed by a Bonferroni post hoc test for multiple comparisons. A *p*-value of less than 0.05 was considered significant. * $p < 0.05$ vs. control, ## $p < 0.01$ vs. AM, *** $p < 0.001$ vs. control, ### $p < 0.001$ vs. AM.

2.3. TEB Exposure Increases Immune Cells' Infiltration Induced by AM

To identify the origin of M1 and M2 marker-positive cells in the myocardium, immunofluorescence is employed to label CD68, a specific cell-surface marker for macrophages, along with iNOS or Arg-1. An increased number of $CD68^+$ $iNOS^+$ double-positive cells were detected in the AM group (Figure 3C,I), as compared to the control (Figure 3A,I, $p < 0.0001$). TEB exposure strongly increased $CD68^+$ $iNOS^+$ double-positive cells in both control (Figure 3B,I, $p = 0.005$) and AM group (Figure 3D,I, $p = 0.0341$). No differences were found in the number of $CD68^+$ $Arg\text{-}1^+$ double-positive cells among all groups (Figure 3E–H,J). RT-PCR analysis was employed to evaluate the CD11b (Figure 3K) and CD45 (Figure 3L) mRNA expression. Samples from the AM group showed increased CD11b (Figure 3K) and CD45 (Figure 3L) levels as compared to control ($p < 0.0001$). TEB exposure strongly increased its expression in both the control ($p = 0.0343$ and $p = 0.0479$, respectively) and AM group (Figure 3K, $p = 0.0015$ and 3L, $p = 0.0041$).

2.4. TEB Exposure Enhances Pro-Inflammatory Markers Induced by AM

To evaluate the effect of TEB exposure on the pro-inflammatory macroenvironment, levels of pro- and anti-inflammatory cytokines were evaluated. Samples from the AM group showed increased levels of TNF-α (Figure 4A, $p < 0.0001$), IL-6 (Figure 4B, $p < 0.0001$), IL-17 (Figure 4C, $p < 0.0001$) and IL-2 (Figure 4D, $p < 0.0001$) and reduced levels of IL-10 (Figure 4E, $p < 0.0001$) and IL-4 (Figure 4F, $p < 0.0001$), as compared to control. TEB exposure strongly increased pro-inflammatory cytokine expression in both control (Figure 4A $p = 0.0090$, Figure 4B $p = 0.0056$, Figure 4C $p = 0.0033$, Figure 4D $p = 0.0040$, respectively) and AM group (Figure 4A $p = 0.0016$, Figure 4B $p = 0.0013$, Figure 4C $p = 0.0149$, Figure 4D $p < 0.0001$, respectively). Additionally, it reduced the expression of the anti-inflammatory mediators (Figure 4E $p = 0.0297$ vs. control and $p = 0.0098$ AM, respectively, Figure 4F $p < 0.0001$ control and $p = 0.0193$ AM, respectively).

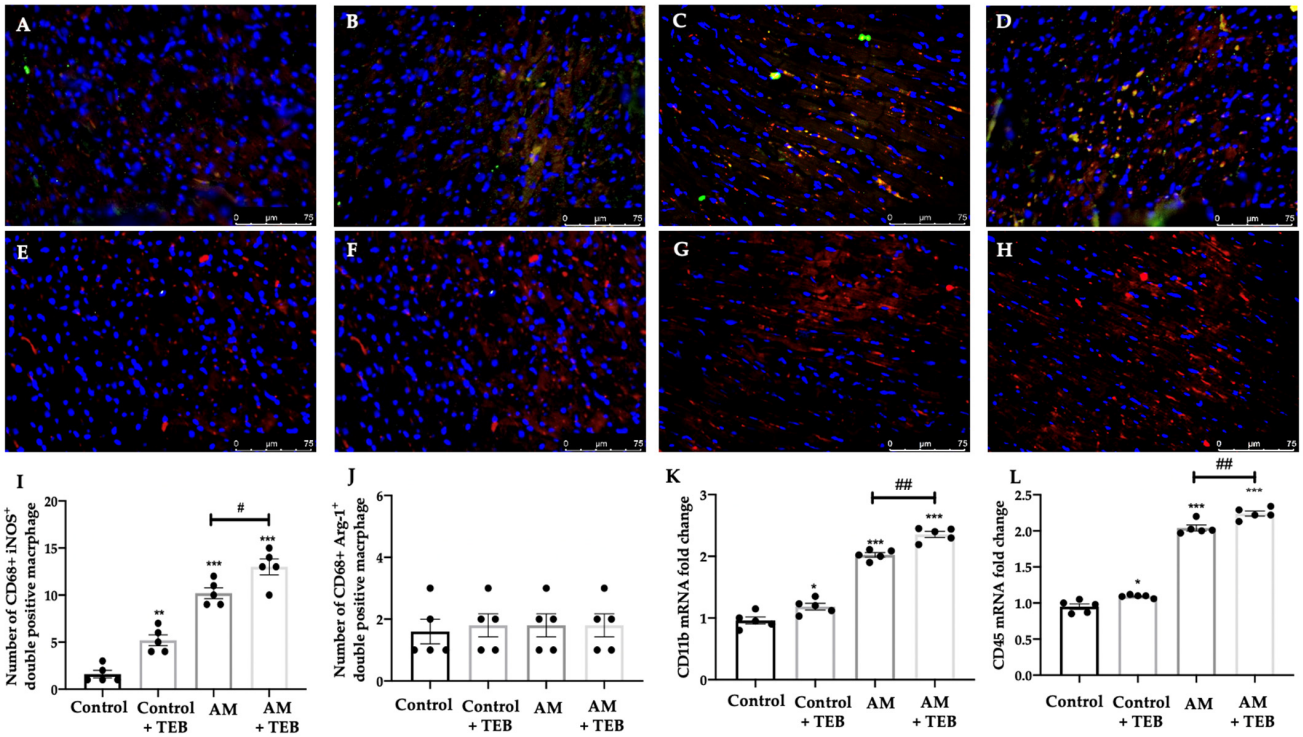

Figure 3. Effect of TEB exposure immune cells' infiltration induced by AM: Double immunofluorescence analysis of CD68 and iNOS of: (**A**) control, (**B**) control + TEB, (**C**) AM, (**D**) AM + TEB groups showed that TEB exposure increased number of CD68+ iNOS+ double-positive cells (**I**). Double immunofluorescence analysis of CD68 and Arg-1 of: (**E**) control, (**F**) control + TEB, (**G**) AM, (**H**) AM + TEB groups showed no differences in the number of CD68+ Arg-1+ double-positive cells (**J**) among the groups. RT-PCR analysis of: (**K**) CD11b, (**L**) CD45 expression showed increased levels of both mRNAs after TEB exposure. Results were analyzed by one-way ANOVA, followed by a Bonferroni post hoc test for multiple comparisons. A *p*-value of less than 0.05 was considered significant. * $p < 0.05$ vs. control, # $p < 0.05$ vs. AM, ** $p < 0.01$ vs. control, ## $p < 0.01$ vs. AM, *** $p < 0.001$ vs. control.

2.5. TEB Exposure Increased Prooxidants Species and Reduced Antioxidant Enzyme Levels Induced by AM

Twenty-one days post AM induction, a significantly higher release of all evaluated prooxidant markers (O_2^-, H_2O_2, NO_2^- and TBARS) was found in the AM group as compared to control (Figure 5A $p < 0.0001$, Figure 5B $p = 0.0043$, Figure 5C $p < 0.0001$ and 5D $p < 0.0001$, respectively). TEB exposure significantly increased all these parameters in both control (Figure 5A $p = 0.0404$, Figure 5B $p = 0.0278$, Figure 5C $p = 0.0261$ and Figure 5D $p = 0.0181$, respectively) and AM groups (Figure 5A $p < 0.0001$, Figure 5B $p = 0.0472$, Figure 5C $p = 0.0029$ and Figure 5D $p = 0.0046$, respectively). Additionally, we evaluated the activity of superoxide dismutase (SOD) and catalase (CAT) enzymes and glutathione (GSH) levels. In AM group SOD (Figure 5E, $p < 0.0001$) and CAT (Figure 5F, $p < 0.0001$) activities were found to be decreased, as compared to control and GSH (Figure 5G, $p < 0.0001$) levels. TEB exposure significantly increased all these activities and levels in both control (Figure 5E $p = 0.0114$, Figure 5F $p = 0.0261$ and Figure 5G $p = 0.0296$, respectively) and AM (Figure 5E $p < 0.0001$, Figure 5F $p = 0.0393$ and Figure 5G $p = 0.0360$, respectively) groups.

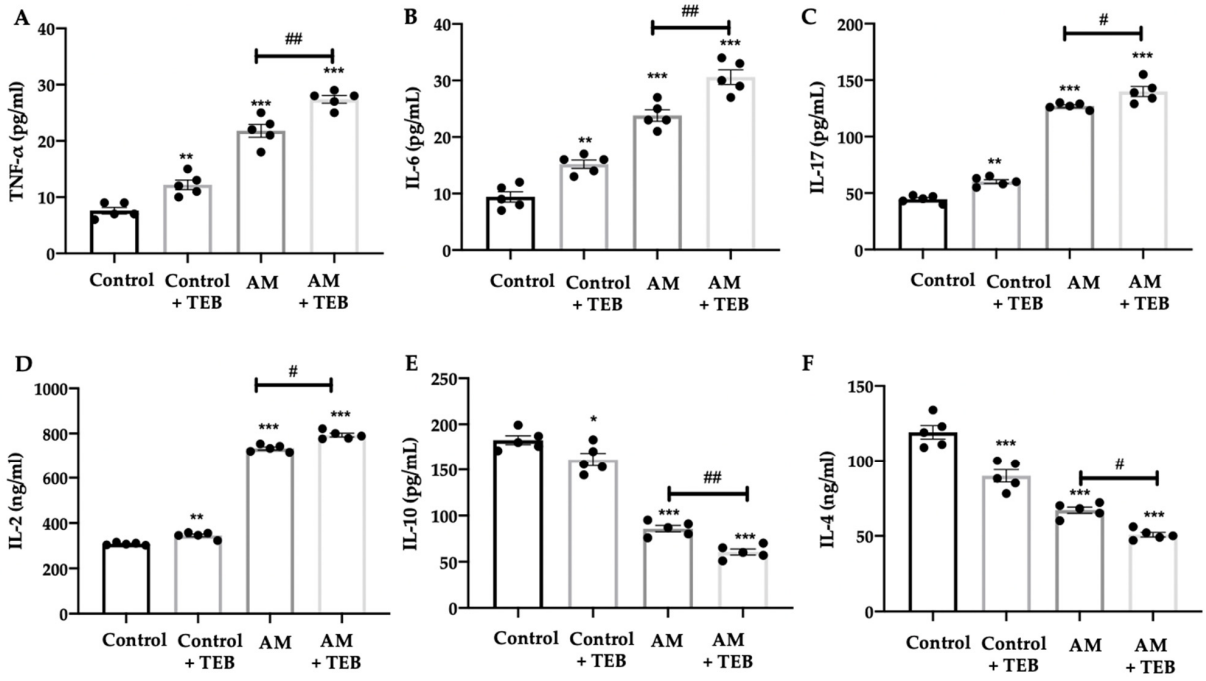

Figure 4. Effect of TEB exposure on pro and anti-inflammatory mediators: ELISA analysis of (**A**) TNF-α, (**B**) IL-6, (**C**) IL-17, (**D**) IL-2 showed that TEB exposure increased levels while reduced (**E**) IL-10 and (**F**) IL-4 expression. Results were analyzed by one-way ANOVA, followed by a Bonferroni post hoc test for multiple comparisons. A *p*-value of less than 0.05 was considered significant. * $p < 0.05$ vs. control, # $p < 0.05$ vs. AM, ** $p < 0.01$ vs. control, ## $p < 0.01$ vs. AM, *** $p < 0.001$ vs. control.

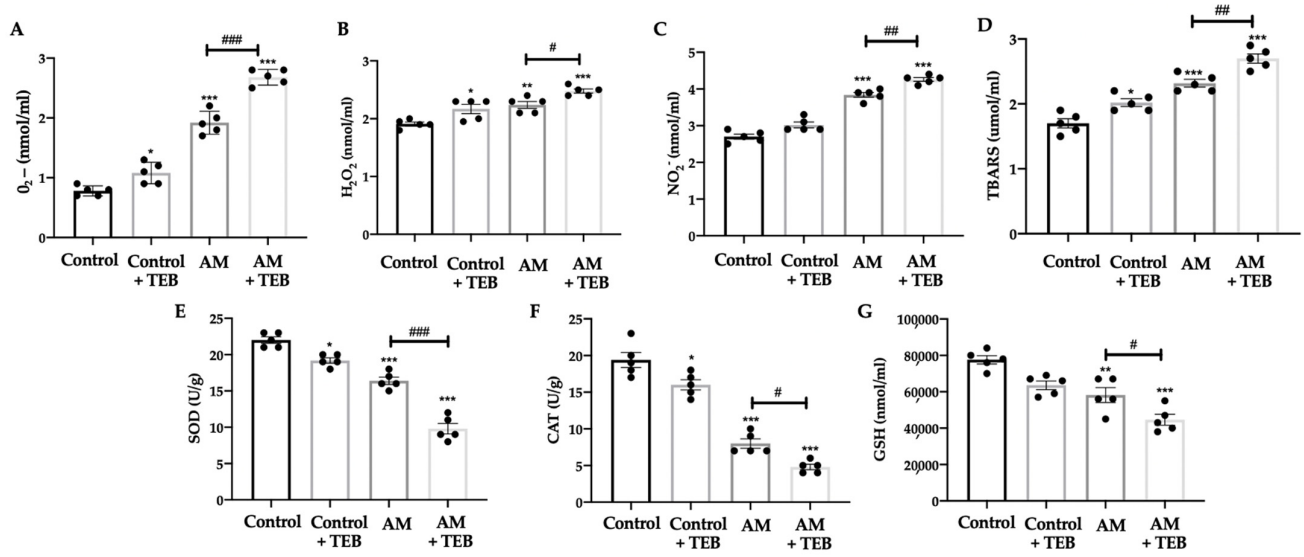

Figure 5. Effect of TEB exposure on oxidative stress parameters activated by AM: (**A**) superoxide anion radical (O_2^-), (**B**) hydrogen peroxide (H_2O_2), (**C**) nitrites (NO_2^-), and (**D**) thiobarbituric acid reactive substances (TBARS) levels were found to be increased after TEB exposure. Moreover, (**E**) superoxide dismutase (SOD) and (**F**) catalase (CAT) activities and (**G**) glutathione (GSH) levels were found to be reduced in the AM + TEB group. Results were analyzed by one-way ANOVA, followed by a Bonferroni post hoc test for multiple comparisons. A *p*-value of less than 0.05 was considered significant. * $p < 0.05$ vs. control, # $p < 0.05$ vs. AM, ** $p < 0.01$ vs. control, ## $p < 0.01$ vs. AM, *** $p < 0.001$ vs. control, ### $p < 0.001$ vs. AM.

2.6. TEB Exposure Elevates the NOX-4- TGFβ1-Smads Expressions Induced by AM

Western blot analysis showed increased NOX-4 (Figure 6A, $p = 0.0045$) and TGFβ1 (Figure 6B, $p = 0.001$) in samples collected from the AM group as compared to control. TEB exposure strongly increased expression in both control (Figure 6A,B $p = 0.0323$) and AM (Figure 6A $p = 0.0108$ and Figure 6B $p = 0.0421$) groups. Western blot and RT-PCR analysis showed an increased phosphorylation of Smad3 in AM group, as compared to control (Figure 6C $p < 0.0001$, and Figure 6D $p < 0.0001$). Additionally, TEB significantly increased p-Smad3 expression in AM + TEB group (Figure 6C $p < 0.0001$, and Figure 6D $p = 0.0002$), as compared to the AM animals. We also evaluated Smad2 phosphorylation. Western blot and RT-PCR analysis showed an increased phosphorylation of Smad2 in AM group, as compared to control (Figure 6E $p < 0.0001$, and Figure 6F $p < 0.0001$). Additionally, TEB significantly increased p-Smad2 expression in AM + TEB group (Figure 6E $p < 0.0001$, and Figure 6F $p < 0.0001$), as compared to the AM animals.

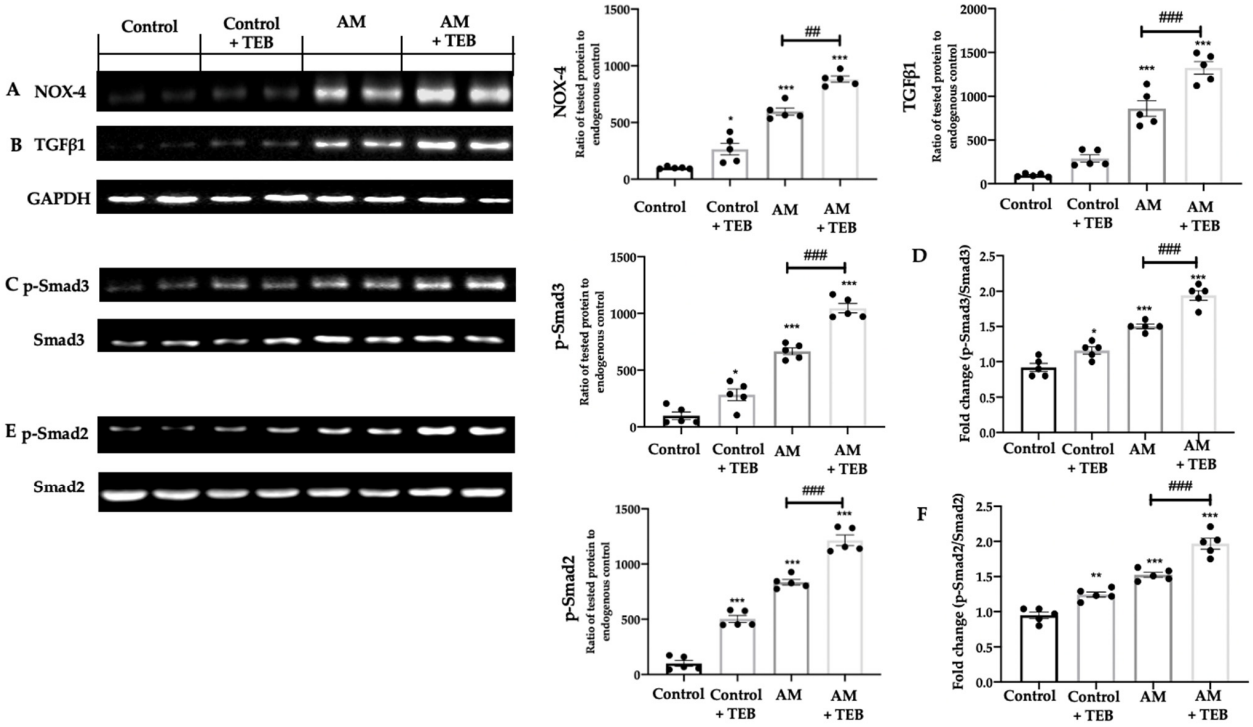

Figure 6. Effect of TEB exposure on NOX-4- TGFβ1-Smads expressions induced by AM: Western blot analysis of: (**A**) NOX-4, (**B**) TGFβ1 expression showed that TEB exposure increased both protein levels. Western blot (**C**) and RT-PCR analysis (**D**) of p-Smad3 showed that TEB exposure increased the p-Smad3/Smad3 ratio. Western blot (**E**) and RT-PCR analysis (**F**) of p-Smad2 showed that TEB exposure increased the p-Smad2/Smad2 ratio. Results were analyzed by one-way ANOVA, followed by a Bonferroni post hoc test for multiple comparisons. A *p*-value of less than 0.05 was considered significant. * $p < 0.05$ vs. control, ** $p < 0.01$ vs. control, ## $p < 0.01$ vs. AM, *** $p < 0.001$ vs. control, ### $p < 0.001$ vs. AM.

2.7. TEB Exposure Aggravates Myocardial Fibrosis and Collagen Deposition Induced by AM

Myocardial fibrosis was evaluated by Masson's Trichrome staining. Control + TEB group showed and increased fibrotic area (Figure 7B,E, $p = 0.0171$), as compared to the control group (Figure 7A,E). AM group showed and increased fibrosis (Figure 7C,E, $p < 0.0001$), as compared to control, and TEB exposure significantly increased it (Figure 7D,E, $p < 0.0001$). There was a statistical difference between AM and AM + TEB groups (Figure 3E, $p < 0.0001$). Western blot and RT-PCR analysis was employed to evaluate changes in Col1a1 (Figure 7F,H) and Col3a1 (Figure 7G,I) expression. TEB exposure significantly increased in both control animals (Figure 7F, $p = 0.0153$, Figure 7H $p = 0.0012$ and Figure 7G, $p = 0.0049$, Figure 7I

$p < 0.0001$). AM group showed a significant increase in Col1a1 (Figure 7F, $p < 0.0001$ and Figure 7H $p < 0.0001$) and Col3a1 (Figure 7G, $p < 0.0001$ and Figure 7I $p < 0.0001$) expression, as compared to control. Additionally, TEB significantly increased Col1a1 (Figure 7F, $p = 0.0009$ and Figure 7H $p = 0.0005$) and Col3a1 (Figure 7G, $p = 0.0362$ and Figure 7I $p < 0.0001$) in AM + TEB group, as compared to the AM animals.

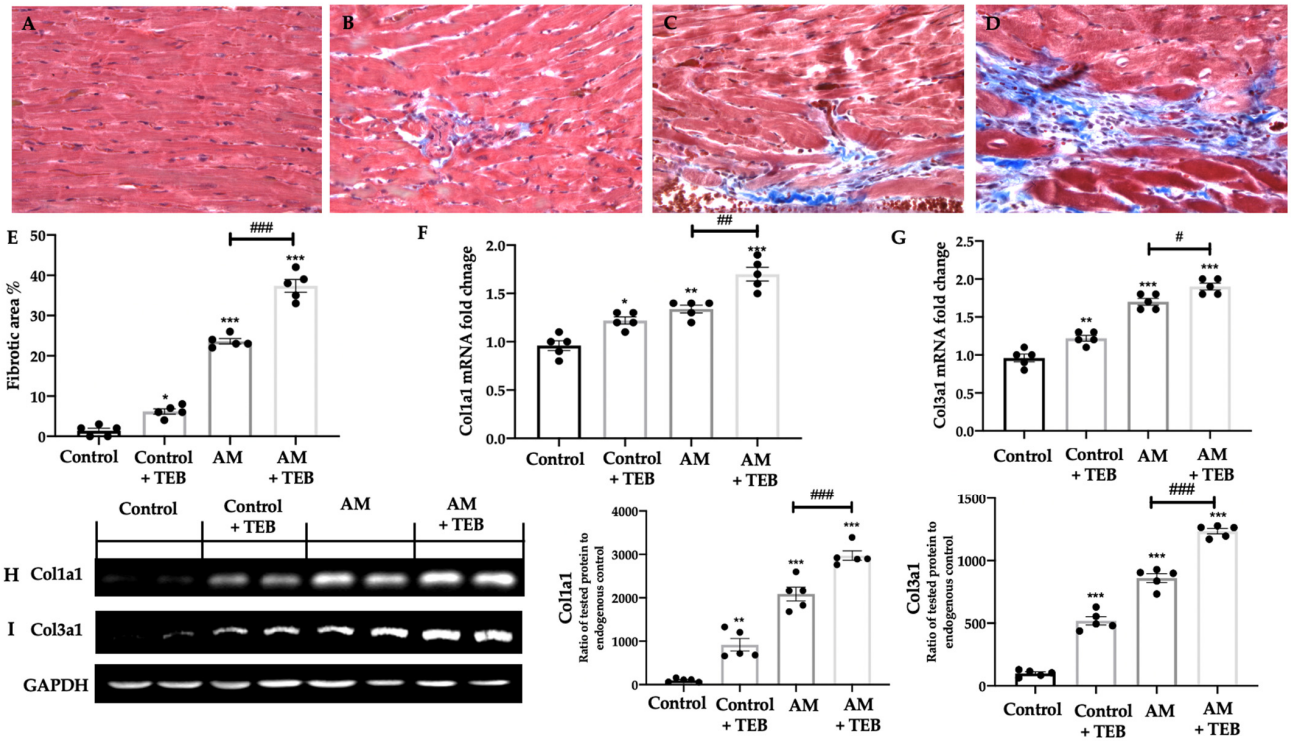

Figure 7. Effect of TEB exposure on fibrosis induced by AM: Masson 's Trichrome staining of: (**A**) control, (**B**) control + TEB, (**C**) AM, (**D**) AM + TEB showed that TEB exposure increased the (**E**) fibrotic area; RT-PCR analysis of: (**F**) Col1a1, (**G**) Col3a1 levels and Western blot analysis (**H**) Col1a1, (**I**) Col3a1 levels showed that TEB exposure increased both. Results were analyzed by one-way ANOVA, followed by a Bonferroni post hoc test for multiple comparisons. A *p*-value of less than 0.05 was considered significant. * $p < 0.05$ vs. control, # $p < 0.05$vs. AM, ** $p < 0.01$ vs. control, ## $p < 0.01$ vs. AM, *** $p < 0.001$ vs. control, ### $p < 0.001$ vs. AM.

3. Discussion

Myocarditis is defined as inflammation of the myocardium that can progress to inflammatory cardiomyopathy when there is associated cardiac remodeling due to chronic inflammation. Rats with AM experience significant alterations in the structure of their heart muscle, characterized by the extensive infiltration of inflammatory cells. These changes ultimately lead to remodeling of the heart and the development of DCM. The underlying mechanisms of this disease are highly intricate and have not been completely understood. Nonetheless, it is established that the overproduction of reactive oxygen species (ROS) followed by oxidative stress triggers the discharge of inflammatory cytokines and chemokines that prompt the movement of leukocytes towards the heart tissue. Furthermore, oxidative stress can lead to the demise of cardiomyocytes via necrosis or apoptosis. This paper focused on the effect of chronic exposure to TEB on AM, analyzing immune cells' recruitment, inflammation, fibrosis, oxidative stress and tissue death.

In our studio, AM rats showed morphometric alterations such as enlargement of the heart, characterized by an elevated Hw/Bw ratio. The cardiotoxic effect of myocarditis was further established by elevated levels of CPK, CK-MB, cTnI and cTnT. Additionally, the AM-rats exhibited high systolic blood pressure and an increased heart rate. Other investigations utilizing the AM model have reported analogous outcomes [13]. The exposure to TEB

resulted in increasing SBP and HR that typically follows myocarditis. Additionally, we observed increased cardiotoxicity in animals exposed to TEB, as shown by the increased levels of CPK, CK-MB, cTnT and cTnI. Histologically, exposure to TEB resulted in modifications to the cardiac architecture. In particular, we observed contraction band necrosis, which results in sarcolemmal rupture, an increased number of apoptotic cells and increased inflammatory infiltration caused by myocarditis [14]. Upon activation, both innate immune cells and cardiac cells release a variety of cytokines, chemokines, interferons, and alarmins. These signaling molecules contribute to the continued activation and recruitment of innate immune cells to the heart, including mast cells, neutrophils, dendritic cells, monocytes, and macrophages [15–18]. Macrophages, being highly adaptable and flexible cells, can differentiate into two distinct subsets in response to signals from the surrounding microenvironment. These subsets include the classically activated macrophages, known as M1, and the alternatively activated macrophages, referred to as M2 [19]. M1 macrophage subtype releases a range of proinflammatory cytokines, including IL-6, TNF-α, and MCP-1. These cytokines elicit antimicrobial, tumoricidal, and proinflammatory effects. In contrast, IL-4 and/or IL-13 frequently polarize macrophages into the M2 phenotype, which then secretes abundant levels of anti-inflammatory cytokines, including IL-10 [20–22]. M2 macrophages have been recognized as reparative cells that possess tissue-restorative effects in certain inflammatory conditions, including AS, diabetic retinopathy, and colitis [23–25]. TEB exposure strongly altered the histological structure of the tissue, increasing necrosis, apoptosis and immune cells' infiltration. In particular, we observed the polarization of the recruited macrophages into the M1 phenotype. This polarization, in turn, induced an increased expression of proinflammatory cytokines and reduced anti-inflammatory cytokine levels. A proinflammatory macroenvironment is accompanied by increased oxidative stress in AM [26,27]. The increased generation of ROS occurs within either cardiomyocytes or endothelial cells [28]. This overproduction is enhanced by the NADPH oxidase pathways [29]. Multisubunit enzymes called NADPH oxidases are present in various locations within cardiac cells [30]. The differentiation of cardiac fibroblasts into myofibroblasts relies on NOX-4 [27]. In the present study, a comparable occurrence was noted through the analysis of NOX-4 expression and the oxidative stress in rats. After being triggered, the NADPH oxidase, which is attached to the membrane, commences single-electron transfers to molecular oxygen, leading to the creation of ROS [31]. Our data showed that NOX-4 expression was increased in AM + TEB-exposed rats, as compared to the rats with AM that were not exposed, underling the detrimental effect of TEB exposure on oxidative stress. This upregulation of NOX-4 levels was accompanied by the increase in TGFβ1 protein expression. The release and activation of cytokines, including TGFβ1, is stimulated by ROS [32]. The augmented expression of the profibrotic marker TGF-β1 in cardiac macrophages is linked to cardiac tissue fibrosis in the hearts of rats [33]. TGFβ1 expression is increased in multiple experimental models of cardiac hypertrophy. Additionally, inhibiting the function of TGFβ1 can prevent cardiac interstitial fibrosis [34] that is caused by pressure overload in rats [35]. Nonetheless, TGFβ1 stimulates the expression of NADPH oxidase and promotes the generation of additional ROS [27]. Out of several fibrotic signals, TGFβ1 is considered a crucial fibrogenic mediator. The downstream mediators of TGFβ1-induced fibrosis, namely Smad2 and Smad3, are well-documented. When Smad2 and Smad3 are activated, they stimulate the synthesis of matrix components such as collagens [36].When TGFβ1 binds to TGFβ1 receptors on cardiomyocytes and cardiac fibroblasts, it triggers signaling pathways mediated by Smad [37]. Our results showed increased TGFβ1 expression in animals with AM exposed to TEB and the contemporary Smads activation. In line with this enhanced TGFβ1 pathway, TEB exposure strongly increased heart fibrosis and collagen deposition. In particular, we found increased expression of key structural collagen types, Col1a1 and Col3a1, in the heart muscle with AM.

Overall, our data showed that TEB exposure induces cardiotoxicity in experimental animals, which strongly increased the progression of AM, increasing immune cells' infiltra-

tion, fibrosis and collagen deposition. Additionally, TEB exposure increased inflammation and oxidative stress, aggravating the TGFβ1-Smads pathway.

4. Materials and Methods

4.1. Animals

Sprague Dawley male rats (male, 6 weeks old, 200–220 g) were purchased from Envigo (Milan, Italy). They were kept in environmentally controlled conditions. The research was authorized by Messina University's Animal Welfare Evaluation Board. All studies were conducted with new Italian legislation (D.Lgs 2014-26), as well as EU rules (EU Directive 2010-63).

4.2. Induction of Autoimmune Myocarditis

Purified porcine cardiac myosin obtained from Sigma Chemical Co. in St. Louis, MO, USA was dissolved in 0.01 M phosphate-buffered saline (PBS) and combined with an equal volume of complete Freund's adjuvant (CFA), supplemented by mycobacterium tuberculosis H37RA (10 mg/mL, Difco) for emulsification. A total of 0.2 mL of the emulsion was subcutaneously injected into the footpads of rats. Following immunization, the rats were exposed to TEB for 21 days [13].

4.3. Experimental Groups

Rats were randomly divided into the following groups (n = 20):

- Control: animals were orally administered with vehicle for 21 days;
- Control + TEB: animals were orally administered with TEB (0.9 mg/Kg) for 21 days;
- AM: rats were subjected to AM as previously described and exposed orally with vehicle every day for 21 days;
- AM + TEB: rats were subjected to AM as previously described and exposed orally with TEB (0.9 mg/Kg) every day for 21 days.

Twenty-one days from the emulsion injection, animals were sacrificed and organs were harvested for histological and molecular analysis.

Route and dose of exposure were based on the literature [10].

4.4. Body and Heart Weight

Bw was monitored during the experiment. At 21 days post-immunization, animals were sacrificed, and hearts were weighted to calculate relative Hw/Bw.

4.5. Blood Pressure and Heart Rate Measurements

Three weeks after immunization, under the influence of isoflurane-induced anesthesia, catheter-tip transducer (ADistrument BP Blood Pressure Transducer for (MLT0699)) was introduced into the left ventricle through the right carotid artery. SBP DBP and HR were analyzed using PowerLab data acquisition system (AD Instruments) and LabChart version 7.2 software on a personal computer [13].

4.6. Histological Analysis

The hearts were harvested and fixed in formalin (10% buffered solution) at room temperature for 24 h. Samples were then dehydrated using a graded series of ethanol, embedded in Paraplast (Sherwood Medical, Mahwah, NJ, USA) [38]. Tissues slices (7 um) were stained with hematoxylin and eosin to perform the histological analysis [39,40]. The sections were scored for myocarditis as follows in blinded (score 0–4) [40,41]: 0, no infiltration or necrosis;1, between 1% and 25% infiltration or necrosis per section; 2, between 26% and 50% infiltration or necrosis per section; 3, between 51% and 74% infiltration or necrosis per section; and 4, between 75% and 100% infiltration or necrosis per section [40]. The sections were examined by light microscopy and all histological evaluations were carried out by our laboratory technician, who did not know the groups' information. Moreover, the area of inflammatory cells was evaluated by image pro plus software (6.0 version), shown

as the ratio of area of inflammatory cells to that of total area. Additionally, sections were also stained with Masson's trichrome to evaluate tissue fibrosis. Collagen accumulation was quantified by the ratio of blue area to total myocardium area. All analyses were performed by an investigator blinded to the group assignments.

4.7. RNA Extraction and cDNA Synthesis

RNeasy kit (Qiagen, Milan, Italy) was employed to extract RNA for real-time polymerase chain reaction (RT-PCR) analysis. Quantification was performed RNA with a spectrophotometer (NanoDrop Lite). An iScript RT-PCR kit (Bio-Rad, Hercules, CA, USA) was used to synthesize first-strand cDNA [42].

4.8. Real-Time PCR

In total, 1 uL of total cDNA was used to perform RT-PCR analysis with the SYBR Green method (Applied Biosystems) [43]. GAPDH and β-actin were employed as an internal control. In addition to biological replicates, three technical replicates were carried out for each target gene. To test for the potential contamination of genomic DNA in the samples, RNA was used as a template for negative controls in all runs.

4.9. Determination of Prooxidants

Superoxide anion radical quantification was based on the reaction of $O2^{-}$ with nitro blue tetrazolium. The protocol included mixing 50 µL of plasma samples and 950 µL of assay mixture, followed by measuring on 550 nm in triplicate every 60 s. Hydrogen peroxide quantification was based on the reaction of phenol red with horseradish peroxidase enzyme. Plasma samples were mixed with phenol red solution and horseradish peroxidase (1:20). Measurements were performed at 610 nm.

Nitric oxide levels were indirectly assessed by measuring nitrite concentration, since NO decomposes rapidly, forming an equal amount of nitrite products. First, 100 µL of PCA (perchloride acid), 400 µL of 20 mM ethylenediaminetetraacetic acid (EDTA), and 200 µL of the plasma sample were mixed, put on ice for 15 min, and centrifuged for 15 min at 6000 rpm. After separating the supernatant, 220 µL K2CO3 was added. Measuring was performed at 550 nm. An index of lipid peroxidation in the plasma samples was estimated indirectly by measuring TBARS. First, TBA extract was made by mixing 800 µL sample and 400 µL trichloroacetic acid (TCA), which was then put on ice for 10 min and centrifuged for 15 min at 6000 rpm. Next, 1% TBA (thiobarbituric acid) in 0.05 NaOH was incubated with the obtained sample at 100 °C for 15 min and after 10 min measured at wavelength of 530 nm [44].

4.10. Antioxidant Enzyme Assay

Tissue samples were lysate and employed to determine the antioxidant enzyme activity. CAT determination was carried out using a mixture of CAT buffer, and 10mM H2O2, with detection taking place at 360 nm. SOD activity was evaluated at 470 nm. Lysate sample was first mixed with carbonate buffer, and then epinephrine was added. The amount of SOD and CAT was expressed as U/g. GSH level was determined with 5,5-dithiobis-6,2-nitrobenzoic acid. GSH extract was made by mixing 100 µL 0.1% EDTA, 400 µL lysate, and 750 µL precipitation solution (1.67 g metaphosphoric acid, 0.2 g EDTA, 30 g NaCl, and filled with distilled water to 100 mL). This was followed by mixing in the vortex machine and extraction on cold ice (15 min) and centrifugation at 4000 rpm (10 min). The level of GSH was measured at 420 nm [44].

4.11. ELISA Analysis

ELISA kits were consumed to measure cardiac enzymes; CPK (ab187396), CK-MB (ab187396), cTnT (ab246529) and cTnI (ab246529) (all obtained from Abcam, Eugene, OR, USA), following the manufacturer's protocols [45]. The concentration of serum cytokines TNF-α, IL-17, IL-10, and IL-6 was determined using ELISA kits (R&D Systems; Minneapolis,

MN, USA). Serum IL-2 and IL-4 were determined by assay kits (Eagle Biosciences, Inc., Amherst, NH, USA).

4.12. Western Blot Analysis

Western blot analysis was performed as previously described [46]. Membranes were probed with one of the following primary antibodies: anti-NOX-4 (PA5-72816), anti-TGFβ1 (Santa Cruz Biotechnology, Heidelberg, Germany, sc-130348), anti-p-Smad3 (cell signaling), anti-p-Smad2 (cell signaling), anti-Smad3 (cell signaling), anti-Smad2 (cell signaling), anti-Col13a1 (Santa Cruz Biotechnology, sc-514601), anti-Col11a1 (Thermo Fisher), in 1 x PBS, 0.1% Tween-20, 5% *w*/*v* non-fat dried milk (PMT) at 4 °C overnight [47,48]. Membranes were incubated with peroxidase-conjugated bovine anti-mouse IgG secondary antibody or peroxidase-conjugated goat anti-rabbit IgG (Jackson ImmunoResearch) [49]. Blots were also incubated with primary antibody against GAPDH (Santa Cruz Biotechnology). Signals were detected with an enhanced chemiluminescence detection system reagent according to the manufacturer's instructions (SuperSignalWest Pico Chemiluminescent Substrate, Pierce) [49].

4.13. Immunofluorescence Analysis

The immunofluorescence analysis was carried out according to previously published methodology [50]. Anti-68 antibody (Santa Cruz Biotechnology) and anti-iNOS antibody (Santa Cruz Biotechnology) and anti-Arg-1 antibody (Santa Cruz Biotechnology) were incubated in a humidified chamber at 37 °C O/N on the sections. After washing with PBS, sections were incubated for 1 h at 37 °C with secondary antibodies, TEXAS RED-conjugated anti-rabbit Alexa Fluor-594 (Molecular Probes, Eugene, OR, USA) and FITC-conjugated anti-mouse Alexa Fluor-488 (Molecular Probes, Eugene, OR, USA). Nuclei were stained by adding 2 µg/mL 40,60-diamidino-2-phenylindole (DAPI; Hoechst, Frankfurt, Germany) in PBS. Slides were then washed with PBS and incubated with a secondary antibody. Specific labeling was identified with an avidin–biotin-peroxidase complex and a biotin-conjugated goat anti-rabbit immunoglobulin G (Vector Lab, Milan, Italy) [51]. Stained sections were observed using a Leica DM6 microscope (Leica Microsystems SpA, Milan, Italy). Each specimen was observed in five random visual fields and the average number of double-positive cells in each specimen was calculated [19].

4.14. TUNEL Assay

Apoptosis was analyzed by a TUNEL assay using a kit (In Situ Cell Death Detection Kit, DBA Italia, Milan, Italy) [52]. TMR red is based on the detection of single- and double-stranded DNA breaks that occur at the early stages of apoptosis. Tissue samples were incubated with the TUNEL reaction mixture that contains TdT and TMR-dUTP. During this incubation period, TdT catalyzed the addition of TMR-dUTP at free 3′-OH groups in single- and double-stranded DNA. After washing, the label incorporated at the damaged sites of the DNA was visualized by fluorescence microscopy.

4.15. Statistical Evaluation

Data are representative of at least three independent experiments and are expressed as the mean ± SEM from N animals/group. Results were analyzed by one-way ANOVA, followed by a Bonferroni post hoc test for multiple comparisons. A *p*-value of less than 0.05 was considered significant. * $p < 0.05$ vs. control, # $p < 0.05$ vs. AM, ** $p < 0.01$ vs. control, ## $p < 0.01$ vs. AM, *** $p < 0.001$ vs. control, ### $p < 0.001$ vs. AM.

Supplementary Materials: The following supporting information can be downloaded at: https://www.mdpi.com/article/10.3390/ijms241411510/s1.

Author Contributions: Conceptualization, S.C. and R.D.P.; investigation, Y.M., A.A. and R.D.; data curation, M.C., R.S. and D.I.; writing—original draft preparation, R.F. and E.G., project administration, R.F. and E.G.; funding acquisition, S.C. and R.D.P. All authors have read and agreed to the published version of the manuscript.

Funding: This research received no external funding.

Institutional Review Board Statement: This study was conducted according to the guidelines of the Declaration of Helsinki and approved by the Institutional Review Board for Animal Care (OPBA) of the University of Messina.

Informed Consent Statement: Not applicable.

Data Availability Statement: The data presented in this study are available on request from the corresponding author.

Conflicts of Interest: The authors declare no conflict of interest.

References

1. Bracamonte-Baran, W.; Cihakova, D. Cardiac Autoimmunity: Myocarditis. *Adv. Exp. Med. Biol.* **2017**, *1003*, 187–221. [CrossRef]
2. Suzuki, J.; Ogawa, M.; Watanabe, R.; Morishita, R.; Hirata, Y.; Nagai, R.; Isobe, M. Autoimmune giant cell myocarditis: Clinical characteristics, experimental models and future treatments. *Expert Opin. Ther. Targets* **2011**, *15*, 1163–1172. [CrossRef] [PubMed]
3. Yilmaz, B.; Terekeci, H.; Sandal, S.; Kelestimur, F. Endocrine disrupting chemicals: Exposure, effects on human health, mechanism of action, models for testing and strategies for prevention. *Rev. Endocr. Metab. Disord.* **2020**, *21*, 127–147. [CrossRef]
4. Lauretta, R.; Sansone, A.; Sansone, M.; Romanelli, F.; Appetecchia, M. Endocrine Disrupting Chemicals: Effects on Endocrine Glands. *Front. Endocrinol.* **2019**, *10*, 178. [CrossRef] [PubMed]
5. De Coster, S.; Van Larebeke, N. Endocrine-disrupting chemicals: Associated disorders and mechanisms of action. *J. Environ. Public Health* **2012**, *2012*, 713696. [CrossRef]
6. Ghannoum, M.A.; Rice, L.B. Antifungal agents: Mode of action, mechanisms of resistance, and correlation of these mechanisms with bacterial resistance. *Clin. Microbiol. Rev.* **1999**, *12*, 501–517. [CrossRef] [PubMed]
7. Bernabo, I.; Guardia, A.; Macirella, R.; Sesti, S.; Crescente, A.; Brunelli, E. Effects of long-term exposure to two fungicides, pyrimethanil and tebuconazole, on survival and life history traits of Italian tree frog (Hyla intermedia). *Aquat. Toxicol.* **2016**, *172*, 56–66. [CrossRef] [PubMed]
8. Fustinoni, S.; Mercadante, R.; Polledri, E.; Rubino, F.; Colosio, C.; Moretto, A. Biomonitoring human exposure to tebuconazole. *Toxicol. Lett.* **2012**, S51. [CrossRef]
9. Schummer, C.; Salquèbre, G.; Briand, O.; Millet, M.; Appenzeller, B.M. Determination of farm workers' exposure to pesticides by hair analysis. *Toxicol. Lett.* **2012**, *210*, 203–210. [CrossRef]
10. Ben Othmene, Y.; Hamdi, H.; Annabi, E.; Amara, I.; Ben Salem, I.; Neffati, F.; Najjar, M.F.; Abid-Essefi, S. Tebuconazole induced cardiotoxicity in male adult rat. *Food. Chem. Toxicol.* **2020**, *137*, 111134. [CrossRef] [PubMed]
11. D'Amico, R.; Gugliandolo, E.; Cordaro, M.; Fusco, R.; Genovese, T.; Peritore, A.F.; Crupi, R.; Interdonato, L.; Di Paola, D.; Cuzzocrea, S.; et al. Toxic Effects of Endocrine Disruptor Exposure on Collagen-Induced Arthritis. *Biomolecules* **2022**, *12*, 564. [CrossRef]
12. Popescu, M.; Feldman, T.B.; Chitnis, T. Interplay Between Endocrine Disruptors and Immunity: Implications for Diseases of Autoreactive Etiology. *Front. Pharmacol.* **2021**, *12*, 626107. [CrossRef]
13. D'Amico, R.; Fusco, R.; Cordaro, M.; Interdonato, L.; Crupi, R.; Gugliandolo, E.; Di Paola, D.; Peritore, A.F.; Siracusa, R.; Impellizzeri, D.; et al. Modulation of NRF-2 Pathway Contributes to the Therapeutic Effects of Boswellia serrata Gum Resin Extract in a Model of Experimental Autoimmune Myocarditis. *Antioxidants* **2022**, *11*, 2129. [CrossRef] [PubMed]
14. Leone, O.; Pieroni, M.; Rapezzi, C.; Olivotto, I. The spectrum of myocarditis: From pathology to the clinics. *Virchows Arch.* **2019**, *475*, 279–301. [CrossRef] [PubMed]
15. Sagar, S.; Liu, P.P.; Cooper, L.T. Myocarditis. *Lancet* **2012**, *379*, 738–747. [CrossRef]
16. Smith, S.; Allen, P. Myosin-induced acute myocarditis is a T cell-mediated disease. *J. Immunol.* **1991**, *147*, 2141–2147. [CrossRef] [PubMed]
17. Palaniyandi, S.S.; Watanabe, K.; Ma, M.; Tachikawa, H.; Kodama, M.; Aizawa, Y. Inhibition of mast cells by interleukin-10 gene transfer contributes to protection against acute myocarditis in rats. *Eur. J. Immunol.* **2004**, *34*, 3508–3515. [CrossRef]
18. Matsui, Y.; Okamoto, H.; Jia, N.; Akino, M.; Uede, T.; Kitabatake, A.; Nishihira, J. Blockade of macrophage migration inhibitory factor ameliorates experimental autoimmune myocarditis. *J. Mol. Cell. Cardiol.* **2004**, *37*, 557–566. [CrossRef]
19. Gao, S.; Zhou, J.; Liu, N.; Wang, L.; Gao, Q.; Wu, Y.; Zhao, Q.; Liu, P.; Wang, S.; Liu, Y.; et al. Curcumin induces M2 macrophage polarization by secretion IL-4 and/or IL-13. *J. Mol. Cell. Cardiol.* **2015**, *85*, 131–139. [CrossRef]
20. Gordon, S.; Martinez, F.O. Alternative activation of macrophages: Mechanism and functions. *Immunity* **2010**, *32*, 593–604. [CrossRef]
21. Mosser, D.M.; Edwards, J.P. Exploring the full spectrum of macrophage activation. *Nat. Rev. Immunol.* **2008**, *8*, 958–969. [CrossRef]

22. Mantovani, A.; Sica, A.; Sozzani, S.; Allavena, P.; Vecchi, A.; Locati, M. The chemokine system in diverse forms of macrophage activation and polarization. *Trends Immunol.* **2004**, *25*, 677–686. [CrossRef]
23. Khallou-Laschet, J.; Varthaman, A.; Fornasa, G.; Compain, C.; Gaston, A.-T.; Clement, M.; Dussiot, M.; Levillain, O.; Graff-Dubois, S.; Nicoletti, A. Macrophage plasticity in experimental atherosclerosis. *PLoS ONE* **2010**, *5*, e8852. [CrossRef]
24. Nishikawa, K.; Seo, N.; Torii, M.; Ma, N.; Muraoka, D.; Tawara, I.; Masuya, M.; Tanaka, K.; Takei, Y.; Shiku, H. Interleukin-17 induces an atypical M2-like macrophage subpopulation that regulates intestinal inflammation. *PLoS ONE* **2014**, *9*, e108494. [CrossRef]
25. Marchetti, V.; Yanes, O.; Aguilar, E.; Wang, M.; Friedlander, D.; Moreno, S.; Storm, K.; Zhan, M.; Naccache, S.; Nemerow, G. Differential macrophage polarization promotes tissue remodeling and repair in a model of ischemic retinopathy. *Sci. Rep.* **2011**, *1*, 1–12. [CrossRef] [PubMed]
26. Tsutsui, H.; Kinugawa, S.; Matsushima, S. Oxidative stress and mitochondrial DNA damage in heart failure. *Circ. J.* **2008**, *72*, A31–A37. [CrossRef] [PubMed]
27. Cucoranu, I.; Clempus, R.; Dikalova, A.; Phelan, P.J.; Ariyan, S.; Dikalov, S.; Sorescu, D. NAD(P)H oxidase 4 mediates transforming growth factor-beta1-induced differentiation of cardiac fibroblasts into myofibroblasts. *Circ. Res.* **2005**, *97*, 900–907. [CrossRef]
28. Zhang, M.; Shah, A.M. ROS signalling between endothelial cells and cardiac cells. *Cardiovasc. Res.* **2014**, *102*, 249–257. [CrossRef] [PubMed]
29. Zuo, L.; Youtz, D.J.; Wold, L.E. Particulate matter exposure exacerbates high glucose-induced cardiomyocyte dysfunction through ROS generation. *PLoS ONE* **2011**, *6*, e23116. [CrossRef]
30. Cave, A.C.; Brewer, A.C.; Narayanapanicker, A.; Ray, R.; Grieve, D.J.; Walker, S.; Shah, A.M. NADPH oxidases in cardiovascular health and disease. *Antioxid. Redox Signal.* **2006**, *8*, 691–728. [CrossRef]
31. Privratsky, J.R.; Wold, L.E.; Sowers, J.R.; Quinn, M.T.; Ren, J. AT1 blockade prevents glucose-induced cardiac dysfunction in ventricular myocytes: Role of the AT1 receptor and NADPH oxidase. *Hypertension* **2003**, *42*, 206–212. [CrossRef]
32. Li, P.F.; Dietz, R.; von Harsdorf, R. Superoxide induces apoptosis in cardiomyocytes, but proliferation and expression of transforming growth factor-beta1 in cardiac fibroblasts. *FEBS Lett.* **1999**, *448*, 206–210. [CrossRef]
33. Shen, J.Z.; Morgan, J.; Tesch, G.H.; Rickard, A.J.; Chrissobolis, S.; Drummond, G.R.; Fuller, P.J.; Young, M.J. Cardiac Tissue Injury and Remodeling Is Dependent Upon MR Regulation of Activation Pathways in Cardiac Tissue Macrophages. *Endocrinology* **2016**, *157*, 3213–3223. [CrossRef]
34. Rosenkranz, S. TGF-beta1 and angiotensin networking in cardiac remodeling. *Cardiovasc Res* **2004**, *63*, 423–432. [CrossRef]
35. Kuwahara, F.; Kai, H.; Tokuda, K.; Kai, M.; Takeshita, A.; Egashira, K.; Imaizumi, T. Transforming growth factor-beta function blocking prevents myocardial fibrosis and diastolic dysfunction in pressure-overloaded rats. *Circulation* **2002**, *106*, 130–135. [CrossRef] [PubMed]
36. Biernacka, A.; Dobaczewski, M.; Frangogiannis, N.G. TGF-beta signaling in fibrosis. *Growth Factors* **2011**, *29*, 196–202. [CrossRef] [PubMed]
37. Dobaczewski, M.; Chen, W.; Frangogiannis, N.G. Transforming growth factor (TGF)-beta signaling in cardiac remodeling. *J. Mol. Cell. Cardiol.* **2011**, *51*, 600–606. [CrossRef] [PubMed]
38. D'Amico, R.; Gugliandolo, E.; Siracusa, R.; Cordaro, M.; Genovese, T.; Peritore, A.F.; Crupi, R.; Interdonato, L.; Di Paola, D.; Cuzzocrea, S.; et al. Toxic Exposure to Endocrine Disruptors Worsens Parkinson's Disease Progression through NRF2/HO-1 Alteration. *Biomedicines* **2022**, *10*, 1073. [CrossRef]
39. Hirakawa, H.; Zempo, H.; Ogawa, M.; Watanabe, R.; Suzuki, J.; Akazawa, H.; Komuro, I.; Isobe, M. A DPP-4 inhibitor suppresses fibrosis and inflammation on experimental autoimmune myocarditis in mice. *PLoS ONE* **2015**, *10*, e0119360. [CrossRef]
40. Zhang, Q.; Hu, L.Q.; Li, H.Q.; Wu, J.; Bian, N.N.; Yan, G. Beneficial effects of andrographolide in a rat model of autoimmune myocarditis and its effects on PI3K/Akt pathway. *Korean J Physiol Pharm.* **2019**, *23*, 103–111. [CrossRef]
41. Hiraoka, Y.; Kishimoto, C.; Kurokawa, M.; Ochiai, H.; Sasayama, S. Effects of polyethylene glycol conjugated superoxide dismutase on coxsackievirus B3 myocarditis in mice. *Cardiovasc. Res.* **1992**, *26*, 956–961. [CrossRef]
42. Di Paola, D.; Capparucci, F.; Lanteri, G.; Crupi, R.; Marino, Y.; Franco, G.A.; Cuzzocrea, S.; Spano, N.; Gugliandolo, E.; Peritore, A.F. Environmental Toxicity Assessment of Sodium Fluoride and Platinum-Derived Drugs Co-Exposure on Aquatic Organisms. *Toxics* **2022**, *10*, 272. [CrossRef]
43. Di Paola, D.; Natale, S.; Iaria, C.; Crupi, R.; Cuzzocrea, S.; Spano, N.; Gugliandolo, E.; Peritore, A.F. Environmental Co-Exposure to Potassium Perchlorate and Cd Caused Toxicity and Thyroid Endocrine Disruption in Zebrafish Embryos and Larvae (Danio rerio). *Toxics* **2022**, *10*, 198. [CrossRef] [PubMed]
44. Draginic, N.D.; Jakovljevic, V.L.; Jeremic, J.N.; Srejovic, I.M.; Andjic, M.M.; Rankovic, M.R.; Sretenovic, J.Z.; Zivkovic, V.I.; Ljujic, B.T.; Mitrovic, S.L.; et al. Melissa officinalis L. Supplementation Provides Cardioprotection in a Rat Model of Experimental Autoimmune Myocarditis. *Oxid. Med. Cell. Longev.* **2022**, *2022*, 1344946. [CrossRef] [PubMed]
45. Mohamed, M.E.; Abduldaium, M.S.; Younis, N.S. Cardioprotective Effect of Linalool against Isoproterenol-Induced Myocardial Infarction. *Life* **2021**, *11*, 120. [CrossRef] [PubMed]
46. Impellizzeri, D.; D'Amico, R.; Fusco, R.; Genovese, T.; Peritore, A.F.; Gugliandolo, E.; Crupi, R.; Interdonato, L.; Di Paola, D.; Di Paola, R.; et al. Acai Berry Mitigates Vascular Dementia-Induced Neuropathological Alterations Modulating Nrf-2/Beclin1 Pathways. *Cells* **2022**, *11*, 2616. [CrossRef]

47. Genovese, T.; Impellizzeri, D.; D'Amico, R.; Fusco, R.; Peritore, A.F.; Di Paola, D.; Interdonato, L.; Gugliandolo, E.; Crupi, R.; Di Paola, R.; et al. Role of Bevacizumab on Vascular Endothelial Growth Factor in Apolipoprotein E Deficient Mice after Traumatic Brain Injury. *Int. J. Mol. Sci.* **2022**, *23*, 4162. [CrossRef] [PubMed]
48. Cordaro, M.; Fusco, R.; D'Amico, R.; Siracusa, R.; Peritore, A.F.; Gugliandolo, E.; Genovese, T.; Crupi, R.; Mandalari, G.; Cuzzocrea, S.; et al. Cashew (*Anacardium occidentale* L.) Nuts Modulate the Nrf2 and NLRP3 Pathways in Pancreas and Lung after Induction of Acute Pancreatitis by Cerulein. *Antioxidants* **2020**, *9*, 992. [CrossRef] [PubMed]
49. Fusco, R.; Cordaro, M.; Siracusa, R.; Peritore, A.F.; Gugliandolo, E.; Genovese, T.; D'Amico, R.; Crupi, R.; Smeriglio, A.; Mandalari, G.; et al. Consumption of Anacardium occidentale L. (Cashew Nuts) Inhibits Oxidative Stress through Modulation of the Nrf2/HO-1 and NF-kB Pathways. *Molecules* **2020**, *25*, 4426. [CrossRef]
50. D'Amico, R.; Fusco, R.; Siracusa, R.; Impellizzeri, D.; Peritore, A.F.; Gugliandolo, E.; Interdonato, L.; Sforza, A.M.; Crupi, R.; Cuzzocrea, S.; et al. Inhibition of P2X7 Purinergic Receptor Ameliorates Fibromyalgia Syndrome by Suppressing NLRP3 Pathway. *Int. J. Mol. Sci.* **2021**, *22*, 6471. [CrossRef]
51. Impellizzeri, D.; Siracusa, R.; Cordaro, M.; Peritore, A.F.; Gugliandolo, E.; D'Amico, R.; Fusco, R.; Crupi, R.; Rizzarelli, E.; Cuzzocrea, S.; et al. Protective effect of a new hyaluronic acid -carnosine conjugate on the modulation of the inflammatory response in mice subjected to collagen-induced arthritis. *Biomed Pharm.* **2020**, *125*, 110023. [CrossRef] [PubMed]
52. Arangia, A.; Marino, Y.; Fusco, R.; Siracusa, R.; Cordaro, M.; D'Amico, R.; Macri, F.; Raffone, E.; Impellizzeri, D.; Cuzzocrea, S.; et al. Fisetin, a Natural Polyphenol, Ameliorates Endometriosis Modulating Mast Cells Derived NLRP-3 Inflammasome Pathway and Oxidative Stress. *Int. J. Mol. Sci.* **2023**, *24*, 5076. [CrossRef] [PubMed]

Disclaimer/Publisher's Note: The statements, opinions and data contained in all publications are solely those of the individual author(s) and contributor(s) and not of MDPI and/or the editor(s). MDPI and/or the editor(s) disclaim responsibility for any injury to people or property resulting from any ideas, methods, instructions or products referred to in the content.